AIAA AVIATION Forum
June 25-29, 2018, Atlanta, Georgia
2018 AIAA/CEAS Aeroacoustics Conference

10.2514/6.2018-3288

An experimental investigation of the effect of bluff body bluntness factor on wake-vortex noise generation

W. Elsahhar*, S. A. Showkat Ali†, R. Theunissen‡
and M. Azarpeyvand§
Faculty of Engineering, University of Bristol, BS8 1TR, UK

An experimental investigation was carried out to study the effect of the bluntness factor of a bluff body on the vortex shedding mechanism in the wake region. Experiments were carried out for a range of bluntness thicknesses. Particle image velocimetry (PIV), dynamic surface pressure and hotwire measurements were taken. PIV showed the bluntness thickness effect on the attachment of the generated vortex to the surface and on the formation length of the vortex. The tonal-coherence between hotwire measurements in the boundary layer upstream of the bluntness and the surface pressure, was shown to be related to downstream location of the vortex core in the time averaged flow field. Velocity fields obtained with PIV indicated a distancing of the vortex formation with increasing bluntness. The study proposes the existence of a critical bluntness value above which the vortex detaches from the bluntness surface and the boundary layer upstream thus produces a lower surface pressure. Below this value the vortex is closer to the blunt surface increasing the vortex interaction surface and the produced surface pressure. However, for smaller bluntness values the relative scaling down of the vortex dominates, introducing a smaller interaction region and lower surface pressure. Both surface pressure reduction schemes suggest effective aeroacoustic noise reduction potential.

Nomenclature

h	Bluff body bluntness thickness, mm
x, y, z	Cartesian coordinates, mm
St	Strouhal number
Re	Reynolds number
L_x	Streamwise length of the bluff body ,mm
L_z	Spanwise length of the bluff body ,mm
U_∞	Freestream flow velocity, m.s^{-1}
U	Total mean flow velocity, m.s^{-1}
U'	Root-mean-square of the flow velocity fluctuations, m.s^{-1}
u	Streamwise mean velocity competent, m.s^{-1}
v	Vertical mean velocity competent, m.s^{-1}
p	Dynamic surface pressure, Pa
ϕ_{uu}	Power spectral density of the flow velocity, dB/Hz
γ^2_{up}	Cross-coherence between the boundary layer velocity and the surface pressure fluctuations
C_p	Surface pressure coefficient
δ	Boundary layer thickness , mm
δ^*	Boundary layer displacement thickness , mm

*Ph.D Student, Department of Mechanical Engineering,(on leave from Ain Shams University), weam.elsahhar@bristol.ac.uk
†Ph.D Student, Department of Mechanical Engineering, ss14494@bristol.ac.uk
‡Senior Lecturer, Department of Aerospace Engineering, r.theunissen@bristol.ac.uk
§Reader in Aeroacoustics, Mechanical Engineering, m.azarpeyvand bristol.ac.uk

I. Introduction

BLUFF bodies and airfoils with blunt trailing edges are widely used in different engineering applications to serve aerodynamic and/or structural purposes.[1–3] In most of these applications, the flow fields associated are prone to vortex shedding in the wake region downstream. A disadvantage occurs when these fluctuating flow fields interact with the surfaces of the solid bodies in flows imposing structural and aeroacoustic noise problems. It is well established that for the vortex shedding to occur at a blunt trailing edge, the bluntness ratio h/δ^* should exceed a critical value of 0.3.[4] Here h represents the blunt trailing edge thickness and δ^* represents the boundary layer displacement thickness at the very trailing edge. An experimental investigation was carried out by Brooks and Hodgson[5] to investigate trailing edge noise generated by an airfoil. The study considered a set of different trailing edge bluntness thicknesses approaching a relatively sharp trailing edge. The vortex shedding related tone was observed in both the near trailing edge surface pressure and the far-field noise spectra for the bluntness ratios exceeding the later critical value. This also agrees with many experimental studies showing that these trailing edge vortex-shedding tones were only observable whenever the critical condition $h/\delta^* > 0.3$ was satisfied.[6–8] Below this critical value the scale of the boundary layer at the trailing edge is much larger than the vortex shedding structures that are limited in scale by the bluntness thickness h. The boundary layer turbulent contribution to the near wake would then mask the relatively weaker tonal fluctuations of the diminished vortex shedding structures. While such understanding is well established for bluntness values below this critical value, the effect of the bluntness factor on the self-noise for bigger bluntness ratios ($h/\delta^* >> 0.3$) has not been investigated in literature as such. Most of the research efforts within this bluntness range are directed more towards vortex shedding suppression using passive/active control methods.[7,9–16] However, a basic understanding of the effect of the bluntness factor on the vortex shedding mechanism in the wake region for these larger bluntness values is still missing. Understanding the self-noise generation mechanisms within that bluntness range is essential to guide the design and implementation of many applications that benefit from the existence of such bluntness values. Therefore, a basic understanding of this effect was attempted in this study. This was done through experimentally investigating a range of relatively blunt bluff bodies ($h/\delta^* >> 0.3$) with different bluntness thickness values (h =6 to 52mm). To investigate the different flow fields associated with the vortex shedding, Particle Image Velocimetry (PIV) measurements were used to produce visualizations of the mean flow field in the near wake region. Moreover, hotwire anemometry yielded both spectral and temporal data representing the dynamic behaviour of the flow in that region and further downstream of the wake. Additionally, surface pressure sensors and hotwire scans provided both pressure gradients and boundary layer profiles upstream of the bluntness respectively. Further on, dynamic surface pressure measurements utilizing specifically designed remote sensors were used to show changes in the surface pressure spectrum upstream of the bluntness. The coherence between hotwire measurements and the dynamic surface pressure data was used to correlate the observed changes in the vortex generation mechanism to the resulted surface fluctuations.

II. Experimental setup

The experiments were performed on five different bluff bodies with trailing edge bluntness thickness h= 6, 10, 20, 30 and 52 mm. A baseline case was considered by infinitely extending the bluff body top surface downstream of the bluntness. A schematic of the bluff bodies used is shown in figure 1. The bluff bodies were made hollow from inside to allow the remote connection of surface pressure sensors to the surface of the top plate of the bluff body. The chord length L_x for all bluff bodies was 350 mm and the span length was L_z = 600 mm. The different bluff bodies were designed to ensure a fully developed turbulent boundary layer upstream of the measurement zone ($-0.25L_x < x < 2.5h$). Each bluff body was fitted with a 3D printed elliptical leading edge upstream to avoid any upstream flow separations. It will be shown that the bluff body length L_x was sufficient to negate upstream influences on the bluff body wake. Moreover, a flow trip was created using a 25 mm wide strip of sand paper, 0.6 mm thick and with a grit roughness of 80. The strip was placed at 0.14 L_x of the leading edge, just off the nose. For each bluff body, measurements were conducted in two different wind tunnels at the University of Bristol (UoB). An open jet wind tunnel was used for hotwire and surface pressure measurements and a closed-circuit low turbulence wind tunnel was used for PIV measurements. The experimental setup and the testing conditions considered for each of the cases are described individually in the following sections.

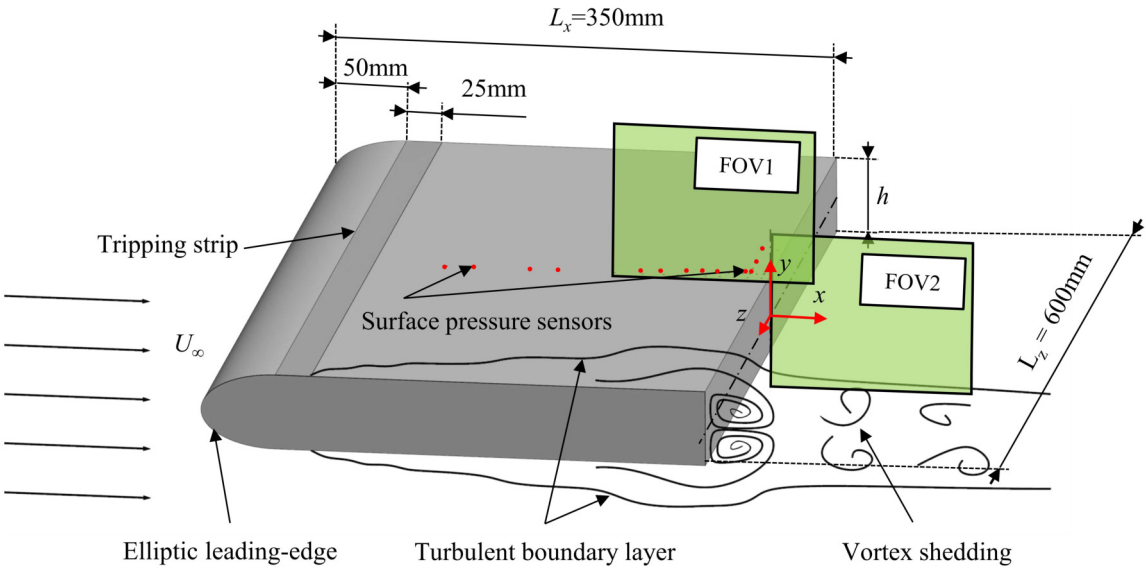

Figure 1. A schematic of the bluff body used in the experimental study

A. Particle image velocimetry measurements setup

The low turbulence closed-circuit wind tunnel facility at the UoB was used for PIV measurements. The wind tunnel has an octagonal cross section with dimensions 0.8 m × 0.6 m × 1 m. The wind tunnel allowed testing at freestream velocities corresponded to a range of $Re_{L_x} = 1.3 \times 10^5$ to 6.9×10^5, with background rms turbulence levels below 0.03 %.[17] The PIV system used was a two component planar PIV system manufactured by Dantec Dynamics. The system consists of a laser to generate a 1 mm thick laser sheet, a particle seeding system and two 2072×2072 pixels CCD cameras, capturing distinct fields of view. The whole bluff body surface was covered with a matt black vinyl sheet to ensure surface continuity and minimise optical reflections toward the PIV cameras. The observed flow regions consisted of, the boundary layer near the trailing edge (FOV1) and the near wake region (FOV2) to cover the surrounding of the vortex formation. FOV1 captured the boundary layer region up to around $1h$ upstream of the bluntness surface, showing the acceleration region upstream of the bluntness. On the other hand, FOV2 started from the bluntness surface up to around one multiple of the vortex size downstream. Having an overlapping region between the frames allowed merging both frames at a common reference line, defined based on the matching of the measured flow parameters. To satisfy the required scales discussed for each FOV, each camera was focused to make each FOV fall in the same (x-y) plane matching a frame size of 161 mm×161 mm. This corresponded to a relative window size of 3.1 h × 3.1 h for the maximum bluntness value. Finally, a series of 1600 image pairs was captured for each FOV. The time resolution of the measurement was limited by a maximum laser sheet triggering rate of 15 Hz. The resulted images were then analysed using the software DynamicStudio provided by the PIV system manufacturer Dantec. An iterative cross-correlation process was applied to the image pairs to result in a velocity vector map. This was applied using a final interrogation window of 16 × 16 pixles with a 50% window overlap, resulting in a final vector spacing of 0.1 h for the minimum bluntness studied.

B. Hotwire anemometry and surface pressure measurements setup

The hotwire and surface pressure measurements were carried out in the open jet wind tunnel at the UoB. The wind tunnel has a circular section with a diameter of 1.1 m. The wind tunnel allowed tests to be performed at a range of freestream velocities ($2.3 \times 10^5 \leq Re_{L_x} \leq 4.6 \times 10^5$).

1. *Surface pressure measurements*

To better understand the relation between the vortex shedding and the boundary layer upstream of the bluntness, both static and dynamic surface pressure measurements were performed for each bluntness case. Pressure taps made out of brass tubes with an internal diameter of 0.6 mm were flush mounted to the surface of the top plate of each bluff body. The pressure taps were distributed along the centre line of the top plate. The static pressure taps covered the region $-0.66 < x/L_x < -0.02$ and the dynamic pressure taps covered the region $-0.23 < x/L_x < -0.01$. Afterwards, 0.4 mm holes were drilled in the vinyl sheet covering the bluff body aligned to the centre of each pressure tap. The miniature diameter of the holes produced a minimal effect on the turbulent flow field and a negligible averaging effect on the measured pressure value due to the minimal area of the sensor. The brass tubes were then remotely connected to either static or dynamic pressure sensors using flexible silicon tubes.

Figure 2 shows a schematic of the remote sensor used for dynamic surface pressure measurements. The remote sensors consisted of a brass pipe fitted in a U shaped slot on the surface of a metal base. Another metal section is placed on the top as to fit the miniature microphone (Panasonic WM-61A). Aligned with the centre of the microphone's pin hole, is another drilled pin hole connecting it to the surface of the brass pipe. At that point on the brass tube surface, a slit was made to connect the whole path from the microphone to the pipe. Finally, a flexible tube extension is connected to the other end of the brass pipe to act as an anechoic termination. The calibration of the remote sensors was done using a specifically designed calibration device. The calibration processes produced the transfer functions required to compensate for the dissipative effects and the lag produced by the remote sensors extensions. This allowed dynamic pressure measurements up to a frequency of 9 kHz.

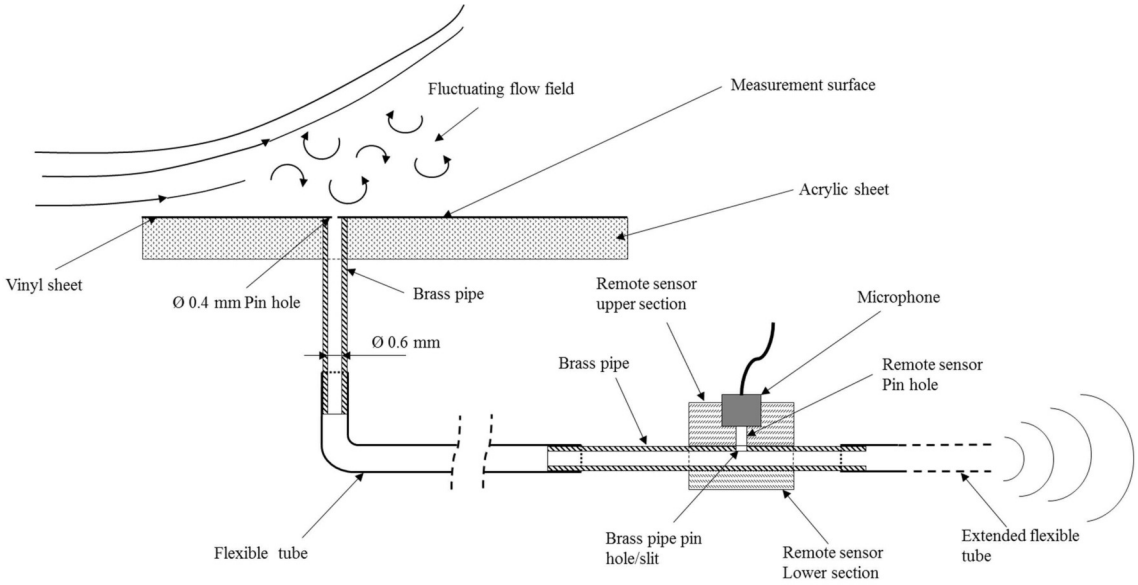

Figure 2. A schematic of the remote sensing configuration used for dynamic surface pressure measurements

For the static pressure sensing, the pressure taps were connected to 16 channels of the static pressure scanner μDAQ2-32DTC (by Chell instruments). The scanner provides a pressure measurement accuracy of $\pm 0.25\%$ of the device full scale, set to 1 PSI. The sampling frequency of the measurement was set to 1 kHz. Referencing of the dynamic pressure was done by connecting the differential pressure of a pitot tube to two channels of the pressure scanner. The pitot tube was placed in the midplane of the jet at a distance of 300 mm from the centre to measure the freestream velocity of the jet. For each static pressure measurement, 10000 samples were taken and averaged to produce a single surface pressure value at each point. These values were then used to calculate the surface pressure coefficient C_p along the surface of each bluff body.

2. Hotwire anemometry

A single-wire hotwire probe (Dantec 55P16)with a $5\mu m$ diameter was used for hotwire anemometry in both of the wake flow field and the boundary layer upstream. The hotwire probe was installed on a 2-axis linear traverse system allowing hotwire scans both in streamwise and vertical directions. The hotwire probe output was connected to a Dantec StreamLine Pro constant temperature anemometry (CTA) system. The module applied a low-pass filter of 30kHz to the hotwire signal an then it was sampled by the A/D card at 102 kHz. At total sampling time of $16s$ was considered for each measurement. The system allowed a dynamic range of 0.2 to 100 m.s^{-1}and measurement accuracy of $\pm 0.5\%$ of the full scale.

III. Results and discussion

A. Static surface pressure measurements and hotwire boundary layer velocity profiles

The flow behaviour in the boundary layer upstream associated with each bluntness value is investigated here by observing the surface pressure gradients and boundary layer profiles. Figure 3 shows the change in profiles across the boundary layer of the average velocity measured by the hotwire U and the associated fluctuations U' observed at different locations upstream of the bluntness. The vertical distance from the surface y is normalized by a reference boundary layer thickness δ_0. δ_0 is the boundary layer thickness at a location upstream where it was found to converge to a similar value for all the studied bluntness values. The results are shown for a $Re_{L_x} = 2.3 \times 10^5$. It can be observed that the total flow velocity U near the bluff

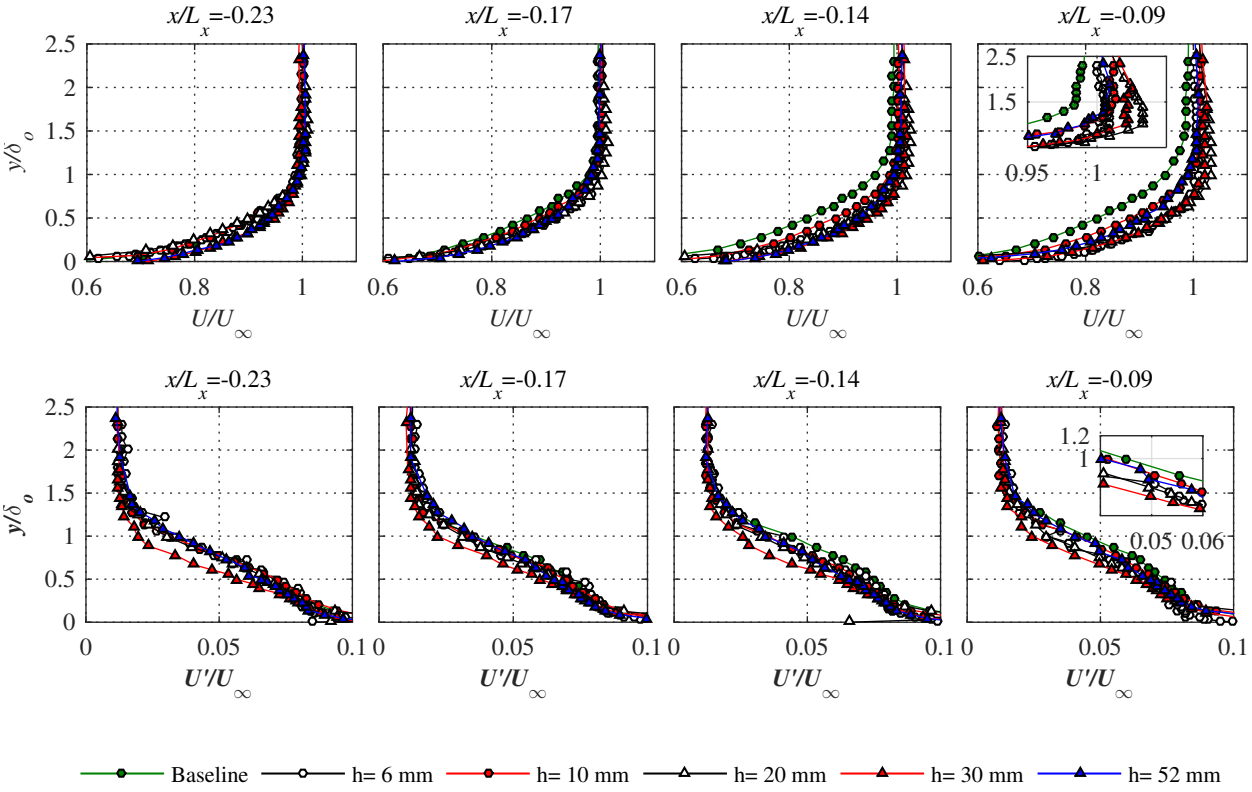

Figure 3. Boundary layer U and U' profiles observed at different locations upstream of the bluntness

body surface tends to accelerate approaching the bluntness compared to the baseline case of an extended plate. However, the intensity of this acceleration was shown to be dependent on the bluntness thickness h. These acceleration values were notably higher for h=20 and 30mm and were much lower for the other cases. Moreover, a decrease was observed in U' values at different streamwise locations approaching the same bluntness values (h=20 and 30mm) and was observed higher for the rest of the studied bluntness values. This

suggests a correlated increase in the mean flow velocity and relative thinning of the boundary layer close to the trailing edge. This can also be observed by looking at the different boundary layer parameters along the bluff body surface as shown in figure 4. The boundary layer displacement thickness δ^* is shown to generally decrease approaching the trailing edge excluding the baseline case and $h = 52$mm case. A relative measure of this gradient can be obtained by observing the change in the boundary layer shape factor $H = \delta^*/\theta$. Where θ is the boundary layer momentum thickness calculated at each location. This ratio gives a measure of the deviation in the behaviour of the boundary layer from the baseline case of a standard turbulent boundary layer with typical H values of 1.3 to 1.4 for turbulent profiles. It is shown here that the shape factor H deviates from the nominal value approaching the trailing edge for the bluntness values h=10, 20 and 30mm. This effect is not equally observed for the bluntness values h=6mm and 52mm, resembling the shape factor H of the baseline case.

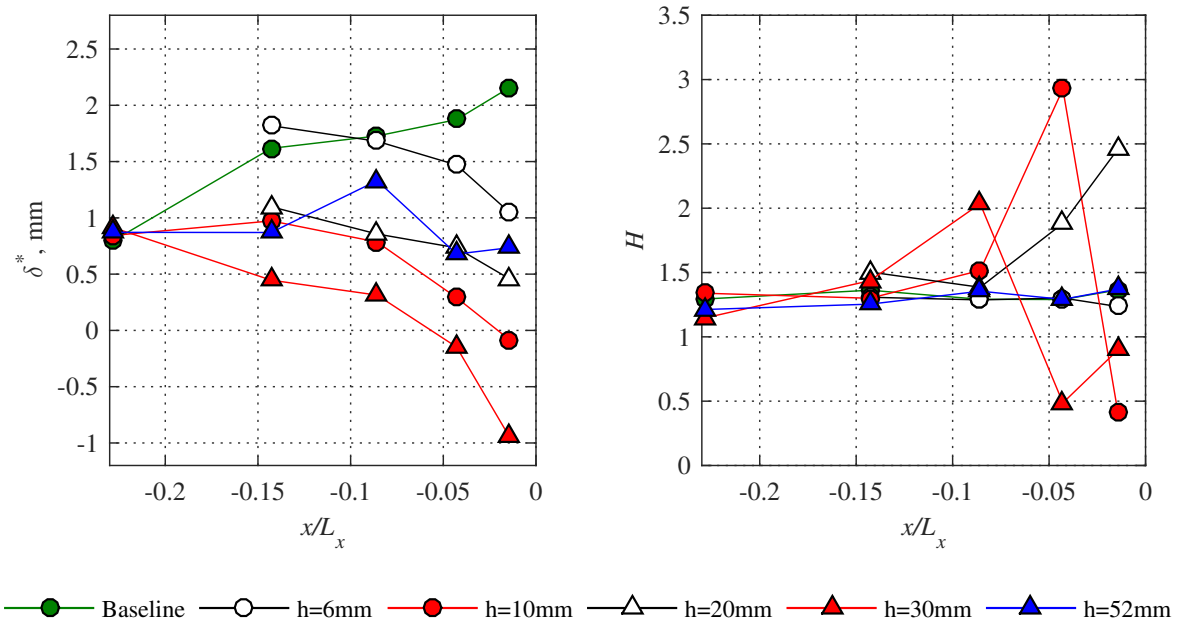

Figure 4. The boundary layer displacement thickness δ^* (left hand side) and the boundary layer shape factor H (right hand side) at different streamwise locations upstream of the bluntness

The later results agreed with what was observed from the distribution of the pressure coefficient C_p upstream of the bluntness. The mean values of C_p are reported in figure 5 and the root-mean square (RMS) C_{prms} values are represented by the error bar around each mean C_p value. For all the bluntness values both the mean and the RMS pressure gradients were noticed to increase approaching the trailing edge, relative to the baseline case. However, the most severe gradients were observed for the h =10 - 30 mm cases. These pressure gradients can be associated with the acceleration of the flow downwards toward the centre of the circulation region at the centreline of the bluntness. Moreover, these flow acceleration gradients are expected to be steeper for bluntness values approaching the range of h=20 to 30mm considering the previous results.

B. PIV results

According to[7] the vortex eye was expected to be around a distance of $1h$ from the bluntness surface with a vortex formation scale of around $1.5h$. The vortex formation scale is defined here as the distance along the symmetry line of the buff body between the rear stagnation point at the bluntness surface and the point downstream at which the mean streamwise component of the velocity $u = 0$.[18] The following results represent a sample of the time-averaged flow field visualised for different bluntness values, obtained from PIV measurements. Figure 6 shows a spatial contour map of the time-averaged normalized v velocity component, plotted along with the flow streamlines deduced from the measured velocity vector field.

Few bluntness thickness correlated effects can be noticed here. First, the formation length of the vortex

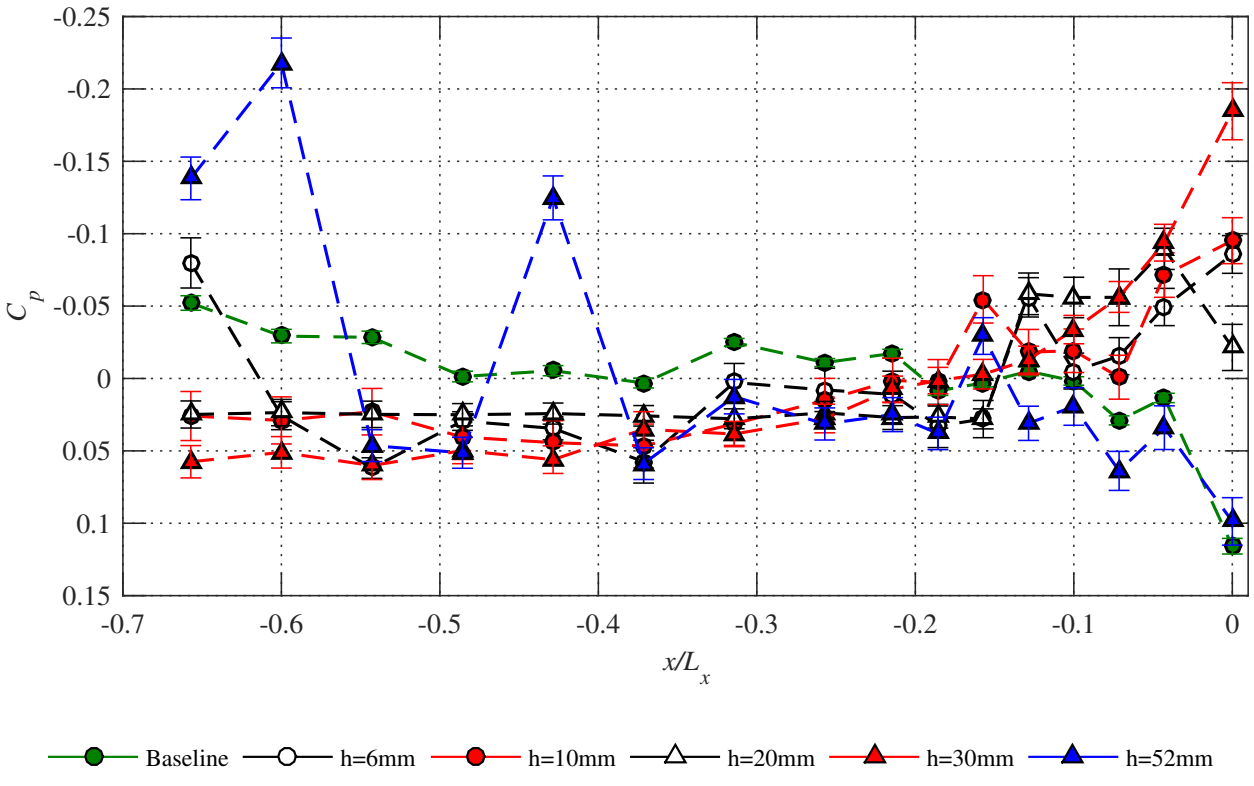

Figure 5. C_p **distribution along the surface of the plate for different bluntness values at** $Re_{L_x} = 2.3 \times 10^5$

increased gradually with the increase in the bluntness thickness from around x/h =0.65 for the h =6mm to more than x/h =1.2 for the 52 mm case. However, a more noticeable effect is the change in the normalized location of the centre of the vortex for each case. It can be seen orderly from figures 6.a to e that the normalized stream vortex centre location is moving further downstream in x direction with the increase in the bluntness value within the range of x/h = 0.4∼0.6 for h=6, 10, 20 and 30 mm, and reaches a value of around x/h =0.9 for the h =52mm case. It can then be clearly seen that the centre of the vortex shifts away from the bluntness surface along with the increase in the bluntness thickness and shifts forward relative to the total formation length. However, this shift in the vortex centre is not linearly proportional to the bluntness value. This is observed as a de-attachment of the main circulation area from the bluntness surface for the h =52mm case that was not observed for smaller bluntness values. Similar trends in the vortex centre locations and scales were also observed at other freestream velocities tested. These results are summarised in figure 7, showing the relation between the bluntness thickness and the vortex formation length in figure 7.a, and between the bluntness thickness and the vortex centre location in figure 7.b. This behaviour suggests the existence of a critical bluntness value above h =30mm at which the main circulation starts to de-attach from the bluntness surface. Another effect that agrees with this behaviour is the steep divergence of the stream lines toward the circulation region that can be noticed for the h =20 and 30 mm cases. On the other hand, this divergence was less prominent for the delayed vortex for h =52mm. These results agree with earlier results showing maximum surface pressure gradients and boundary layer accelerations for h =20 and 30mm where the circulation region is attached to the bluntness surface.

C. Boundary layer velocity spectrum and surface pressure fluctuations coherence

Figure 8 shows the results obtained from hotwire measurements within the boundary layer upstream of the bluntness for each of the bluntness cases. Each subfigure shows a spectral map, representing the PSD of the fluctuating velocity component ϕ_{uu} measured along the boundary layer profile in the normal direction to the freestream flow. The results are shown at different streamwise locations measured upstream of the bluntness.

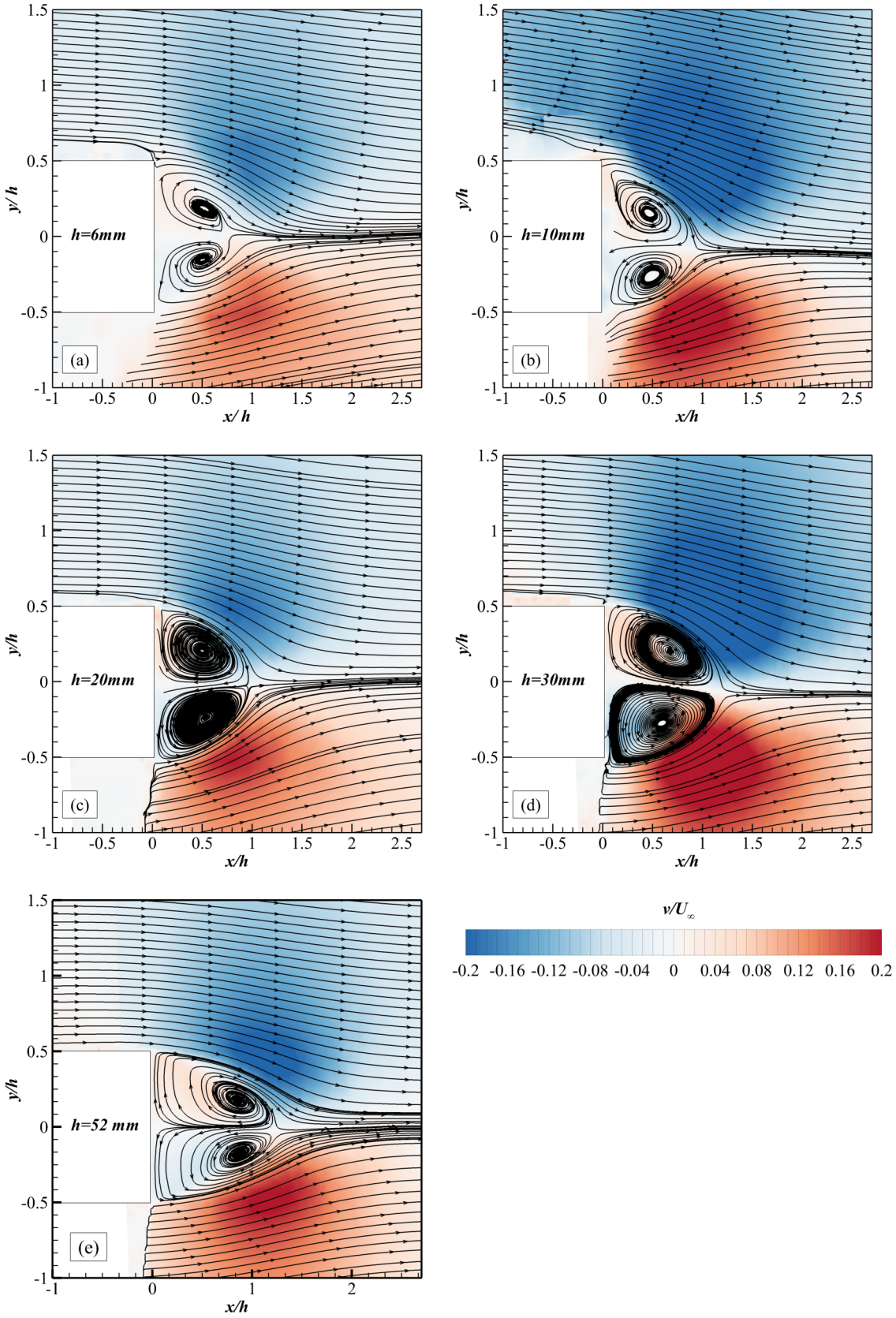

Figure 6. Time-averaged velocity streamline topology and v velocity components contours at $Re_{L_x} = 2.3 \times 10^5$

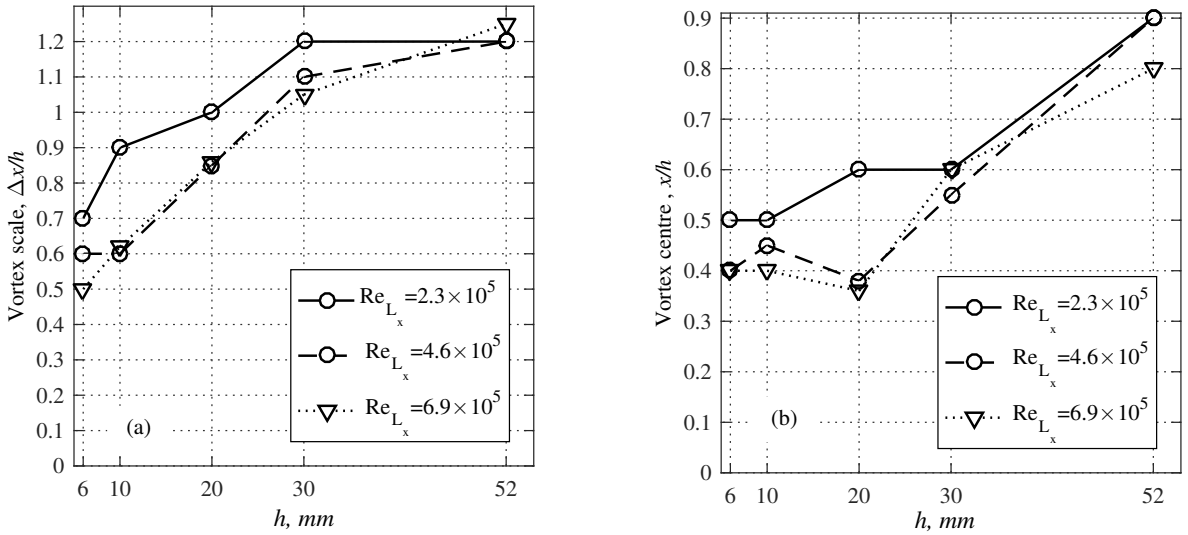

Figure 7. Relation between the bluntness factor h and the vortex scale and location (a)Vortex formation length (b)Vortex centre downstream location

The first case represented is a baseline case of an infinitely extended bluff body. The spectral results are shown in terms of Strouhal number defined based on the bluntness thickness h ($St = f.h/U_\infty$). It can be noticed that the spectral behaviour resembles that of a standard fully developed turbulent boundary layer. For the h =10 mm case, a tonal peak can be noticed around St =0.18. Which becomes noticeable only in the near vicinity of the trailing edge. For the h=30 mm case, a tonal peak can be noticed at St =0.21. However, the amplitude of the peak does not decay rapidly in the upward direction as in the h =10mm case. Instead, further upstream the tone can still be noticed though starting from a different vertical location from the surface. This starting point moves further away from the surface upstream distance. A similar behaviour was also observed for the h = 20 mm case. Finally, for h =52 mm, no tonal peak can be noticed for any streamwise locations in the boundary layer.

Next, simultaneous surface pressure and hotwire measurements were done to correlate surface pressure fluctuations to the flow dynamic behaviour in the boundary layer and along the lip line in the near wake region. The cross-coherence between the boundary layer velocity fluctuations and surface pressure fluctuations is shown in figure 9 as an example of these results. It can be noticed that strong tonal coherence was only shown for the h =20 and 30 mm cases along different streamwise locations. This confirms that the flow interaction between the vortex circulation region and the solid surface of the bluff body was only prominent for the cases where the vortex was attached to the bluntness surface. However, for smaller bluntness values this coherence decays again. Nevertheless, reflecting on the PIV results of these cases another effect related to the scaling down of the vortex circulation region can also be observed. A contraction of the vortex circulation area can be noticed in both vertical and streamwise directions. This agrees with the trend of reduction noticed for near sharp trailing edges considered in previous studies, approaching the range h/δ^* <0.3.[5]

IV. Conclusion

The effect of the bluntness factor of a thick bluff body on the generated vortex shedding dynamics was investigated in this study. It can be concluded that among the range of bluntness values investigated, the tonality of surface pressure fluctuations was found more prominent when the bluntness value approached the range between h =20∼ 30 mm and was less witnessed for either smaller or higher bluntness values. This can be linked to earlier observations of the PIV results which related the change in bluntness to the shift in the centre of the vortex relative to the total formation length. The tonal components observed on the surface of the bluff body close to the trailing edge, might indicate some form of interaction between the main vortex formation and the boundary layer at these locations. For higher bluntness values represented by the h =52 mm case, the vortex centre shifts away downstream from the trailing edge, thus reducing this probable interaction with the boundary layer and the solid surface. This was reflected as a lack of tonal behaviour

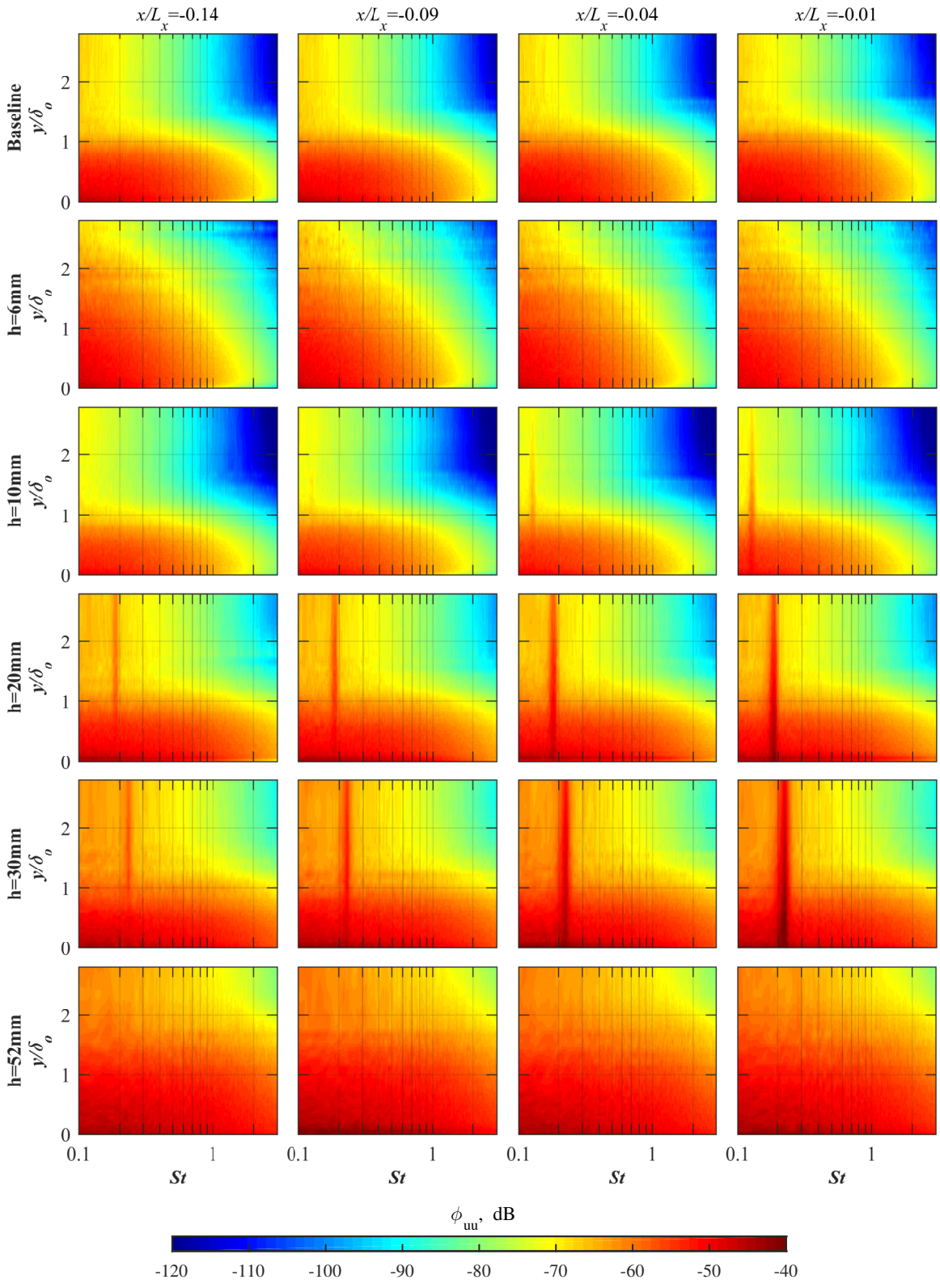

Figure 8. Boundary layer velocity PSD ϕ_{uu} at $Re_{L_x} = 2.3 \times 10^5$

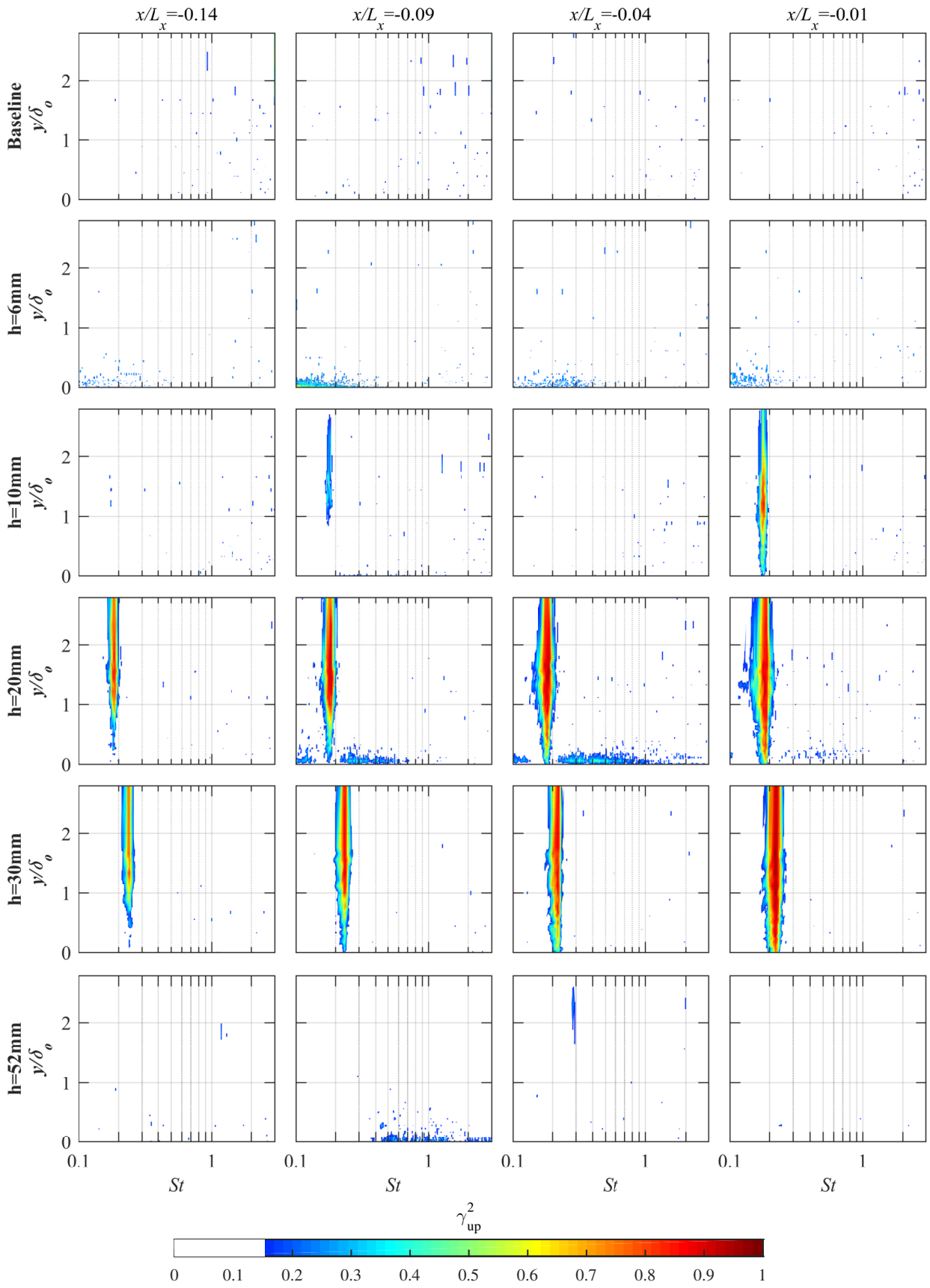

Figure 9. The cross-coherence between the boundary layer velocity and surface pressure fluctuations γ^2_{up} at $Re_{L_x} = 2.3 \times 10^5$

in the boundary layer velocity spectrum and it's coherence with surface pressure fluctuations. Therefore, indicating less potential to produce far-field noise. On the other hand, the reduction in the tonal behaviour associated with bluntness values h <20 mm can be related to the scaling down of the bluntness. Despite that for lower bluntness values the vortex centre is approaching the trailing edge and perceivably introducing more interaction with the boundary layer, the effect of the vortex being scaled down is introducing a more dominant effect. Along with the effect of a slight contraction of the vortex circulation area in the vertical direction. This can be clearly observed in the surface pressure spectrum of the $h = 10$ mm case, where the tonal behaviour was only observed over a small distance upstream of the trailing edge. Finally, the latter observations suggest that a good noise control mechanism might be based on imposing a shift in the vortex centre forcing it to de-attach from the surface of the bluntness.

V. Acknowledgement

The first author (W.E.), would like to thank the Newton-Mosharafa Fund for the financial support offered throughout this research work .

References

[1]Standish, K.J. Van Dam, C., "Aerodynamic Analysis of Blunt Trailing Edge Airfoils," *Journal of Solar Energy Engineering*, Vol. 125, No. 4, 2003, pp. 479 – 487.

[2]Winnemller, T. Van Dam, C., "Design and numerical optimization of thick airfoils including blunt trailing edges," *Journal of Aircraft*, Vol. 44, No. 1, 2007, pp. 232 – 240.

[3]Baker, J., Mayda, E., and Van Dam, C., "Experimental analysis of thick blunt trailing-edge wind turbine airfoils," *Journal of Solar Energy Engineering*, Vol. 128, No. 4, 2006, pp. 422 – 431.

[4]Blake, W. K., *Mechanics of Flow-Induced Sound and Vibration, Volume 1: General Concepts and Elementary Sources*, Academic press, 2017.

[5]Brooks, T. F. and Hodgson, T., "Trailing edge noise prediction from measured surface pressures," *Journal of sound and vibration*, Vol. 78, No. 1, 1981, pp. 69–117.

[6]Herr, M. and Dobrzynski, W., "Experimental investigations in low-noise trailing-edge design," *AIAA journal*, Vol. 43, No. 6, 2005, pp. 1167–1175.

[7]Showkat Ali, S. A., Szoke, M., Azarpeyvand, M., and Ilário, C., "Trailing Edge Bluntness Flow and Noise Control Using Porous Treatments," *22nd AIAA/CEAS Aeroacoustics Conference*, 2016, p. 2832.

[8]Sagrado, A. G., "Boundary layer and trailing edge noise sources," 2008.

[9]Nakamura, Y., "Vortex shedding from bluff bodies with splitter plates," *Journal of Fluids and Structures*, Vol. 10, No. 2, 1996, pp. 147–158.

[10]Lim, H.-C. and Lee, S.-J., "Flow control of a circular cylinder with O-rings," *Fluid Dynamics Research*, Vol. 35, No. 2, 2004, pp. 107–122.

[11]Bearman, P. and Harvey, J., "Control of circular cylinder flow by the use of dimples," *AIAA journal*, Vol. 31, No. 10, 1993, pp. 1753–1756.

[12]Kamps, L., Geyer, T. F., Sarradj, E., and Brücker, C., "Vortex shedding noise of a cylinder with hairy flaps," *Journal of Sound and Vibration*, Vol. 388, 2017, pp. 69–84.

[13]Owen, J. C., Bearman, P. W., and Szewczyk, A. A., "Passive control of VIV with drag reduction," *Journal of Fluids and Structures*, Vol. 15, No. 3-4, 2001, pp. 597–605.

[14]Williams, J. F. and Zhao, B., "The active control of vortex shedding," *Journal of Fluids and Structures*, Vol. 3, No. 2, 1989, pp. 115–122.

[15]Amitay, M., Smith, B. L., and Glezer, A., "Aerodynamic flow control using synthetic jet technology," *AIAA paper*, Vol. 208, 1998, pp. 1998.

[16]Nati, G., Kotsonis, M., Ghaemi, S., and Scarano, F., "Control of vortex shedding from a blunt trailing edge using plasma actuators," *Experimental Thermal and fluid science*, Vol. 46, 2013, pp. 199–210.

[17]Barrett, R., "Design and performance of a new low turbulence wind tunnel at Bristol University," *The Aeronautical Journal*, Vol. 88, No. 873, 1984, pp. 86–90.

[18]Williamson, C. H. K., "Vortex Dynamics in the Cylinder Wake," *Annual Review of Fluid Mechanics*, Vol. 28, No. 1, 1996, pp. 477–539.